Relevance of a glassy nanocrystalline state of Mo_4VO_{14} for its action as selective oxidation catalyst

H. Werner, O. Timpe, D. Herein, Y. Uchida, N. Pfänder, U. Wild and R. Schlögl *

Fritz Haber Institut der Max-Planck Gesellschaft, Faradayweg 4-6, D-14195 Berlin, Germany

H. Hibst

BASF AG, D-67056 Ludwigshafen, Germany

Received 24 January 1997; accepted 30 January 1997

The oxide Mo_4VO_{14}, in its active state, is a partly reduced material with an "amorphous" structure. Temperature-programmed methods reveal that the active lattice oxygen gives rise to a desorption signal at 500 K, which is at the lower end of the temperature window for activity in the selective oxidation of *n*-propanol. The phase is metastable with respect to oxidative crystallisation into isotropic crystals of the title structure occurring at 781 K. Photoemission revealed in the zero bandgap semiconductor oxide of the amorphous state the MO_6 octahedra to be distorted and the oxygen pumping activity to be related to oxidation–reduction cycles of metal d-states situated close to the Fermi energy. Structural studies by XRD and HRTEM showed that the oxygen-pumping state is a nanocrystalline modification of the title structure. The relation of the structural motif to the catalytic function is discussed for this compound and for the whole family of systems in the framework of the theory of glass formation.

Keywords: selective oxidation, molybdates, nanostructured material, lattice oxygen remote-control, HRTEM, UPS, temperature-programmed methods

1. Introduction

The title system has long been known to be active as selective oxidation catalyst [1–3] and substantial efforts were made to optimise its performance by preparative measures [4,5] and by addition of several synergistic agents such as copper molybdates and antimony oxides [6,7]. The analysis of the mode of operation [7,8] of the family of multi-element molybdate catalysts [9], from which the title compound is but one member, has made substantial progress and brought about the relevance of defects, of partial reduction and of modification of connectivity of the octahedral basic structural units. These atomistic details of the general Mars–van Krevelen mechanism were summarised in the remote control hypothesis [10] which accounts for the experimentally well-documented synergistic effect [11] of creating complex oxide derivatives of MoO_3.

In an attempt to rationalise the atomistic details of this hypothesis by experimental means the title system has been chosen for a rigorous functional analysis as it is one of the simple molybdates [12,13] with practical relevance as matrix material for industrial catalyst systems [14,6]. Here we focus on the function of oxygen pumping from the gas phase into the active state of lattice oxygen.

* To whom correspondence should be addressed.

2. Experimental

The catalyst samples were prepared by the method of precipitation of ammonium salts followed by calcination up to 700 K in a slightly oxidising atmosphere (5% oxygen in nitrogen) [5]. Several batches of the material were used throughout this study which differed slightly in their Mo to V content. Two samples contained small amounts of tungsten as partial substitution for molybdenum. All samples were of the same amorphous structure and underwent the same structural phase transition shown below.

Thermal experiments were carried out in a Seiko thermobalance coupled to an Atomica IMR-MS 100 mass analyser which was operated with Xe as primary gas. A variable gas atmosphere with a gas flow rate of 140 ml/min ascertained a controlled chemical environment. A Seiko DSC system was used with the samples heated in air. The TPO experiments were carried out in a vertical glass reactor holding 40 mg catalyst in a 5 mm bed exposed to a gas stream of 150 ml/min which was either pure nitrogen or 5% oxygen in nitrogen. The IMR-MS with Xe and CF_3I as primary gases was used to monitor oxygen, water, NO_x, ammonia and carbon oxides. The linear temperature program was 5 K/min.

Conversion experiments with *n*-propanol/water (azeotrope) were made using the TPO set-up as reactor and the IMR-MS as calibrated detector. 4.45 mmol/(g min) substrate and a tenfold excess of oxygen were fed

over 20 mg catalyst in a total gas stream of 200 ml/min with nitrogen as diluent. Data points were taken after 1 h stationary conversion which was achieved within a few minutes after a parameter change.

The surface analytical experiments were carried out in a combined XPS-UPS-ISS instrument with an EA 200 hemispherical analyser which was operated at 1.0 eV resolution. Mg X-ray radiation (150 W) and He UV radiation were used together with a He 2000.0 eV ion beam (1 μA, raster 2×3 mm, data acquisition at 2 eV analyser resolution within 100 s for "static" ISS). Data were analysed with standard procedures using satellite subtraction, Shirley background subtraction integration and conversion with empirical sensitivity factors suitable for the instrument geometry.

Samples are prepared on a gold substrate as a thin slurry from aqueous suspension. The substrate can be heated to 1000 K in atmospheres from UHV to atmospheric pressure and TDS data can be acquired at linear heating rates of 2 K/s with a mass spectrometer attached to the preparation chamber. Fast insertion into the analyse UHV was possible by an intermediate turbopumping stage ensuring contamination-free transfer within 30 s from atmospheric pressure.

Electron microscopy with EDX analysis was performed with a Phillips CM 200 FEG instrument with a super twin lens and a double tilt specimen holder at 200 keV. The specimen were prepared on holey carbon grids from a slurry of the ground powder prepared by ultrasonication in water. The EDX data for the metals (average 18 ± 2 % V and the rest Mo) ascertained the integrity of the particles used for imaging. The samples are beam-sensitive within 10 min of irradiation leading to a volatilisation of the V-oxygen component and an amorphisation of the matrix structure.

3. Results

3.1. Composition

The bulk elemental composition of the catalyst was analysed for its metal content by XRF. The values found agreed within 1% with those expected. Surface analytical data were obtained both from XPS and from ISS experiments in the as-prepared state and after one cycle of unloading–reloading in 20 mbar oxygen at 723 K for 15 min in the high pressure attachment of the surface analytical machine. Table 1 summarises all relevant data.

XPS reveals that the surface-near volume of the catalyst differs significantly from the average bulk composition in the way that it is enriched in Mo relative to V and O. This enrichment is not removed after one cycle of unloading–loading revealing the partly reduced surface being a genuine property of the catalyst even under reaction conditions which contain gaseous oxygen. The degree of reduction indicates that the catalyst composition is about Mo : O 1 : 2.8 quite within the range of known defect structures of MoO_3 surfaces. The Mo $3d_{5/2}$ single line occurs at 232.14 eV which is a lower value than reported for MoO_3 (232.6 ± 0.25 eV) or for molybdates (aluminium molybdate 233.8 eV).

Table 1
Catalyst composition in at%. The catalyst has the formal stoichiometry Mo_4VO_{14}

Composition	As-prepared	Re-oxidised
bulk V	5.2	–
bulk MO	21.2	–
bulk O	73.6	–
XPS V	5.8	5.1
XPS Mo	24.7	25.8
XPS O	69.5	69.1
XPS reduction degree [a]	0.80	0.89
ISS V	9.1	5.4
ISS Mo	45.0	47.8
ISS O	45.9	46.7
ISS reduction degree [a]	5.36	5.15

[a] The reduction degree is given as deficiency in formula units of oxygen.

With static ISS it was observed that the top atomic layer was much more enriched in Mo and deficient in oxygen as implied by the XPS data. The degree of reduction was so large that the assumption seems adequate that the surface was not oxygen terminated. A Mo termination would imply that the typical surface is not oriented in the (001) cleavage plane but contains a large fraction of prismatic faces exposing a mixture of cations and oxygens. Re-oxidation affects the surface composition slightly, as can be seen from the changed degree of reduction parameter in table 1. The surface after oxygen exposure is by no means covered with oxygen under the conditions of cooling down in oxygen and transfer at 300 K into the UHV of the spectrometer.

The good agreement of the overall ratio V : Mo with the theoretical value indicates that, at all levels of analysis, the sample is a homogeneous ternary oxide with no surface segregation or lateral concentration fluctuation of the ternary element vanadium.

3.2. Thermal analysis

The partially reduced character of the sample as a result of the calcination leading to autoreduction with the evolving ammonia ligands allowed to study the uptake of molecular oxygen under various conditions and so to follow one major function of the catalyst. Figure 1 shows a double oxygen-pump experiment. It can give off and take up oxygen in a partly reversible form. Liberation and oxidation of residual ammonia and of molecular water were observed with the first weight loss accounting for part of the imperfect reversibility. The kinetics of bulk oxygen desorption and

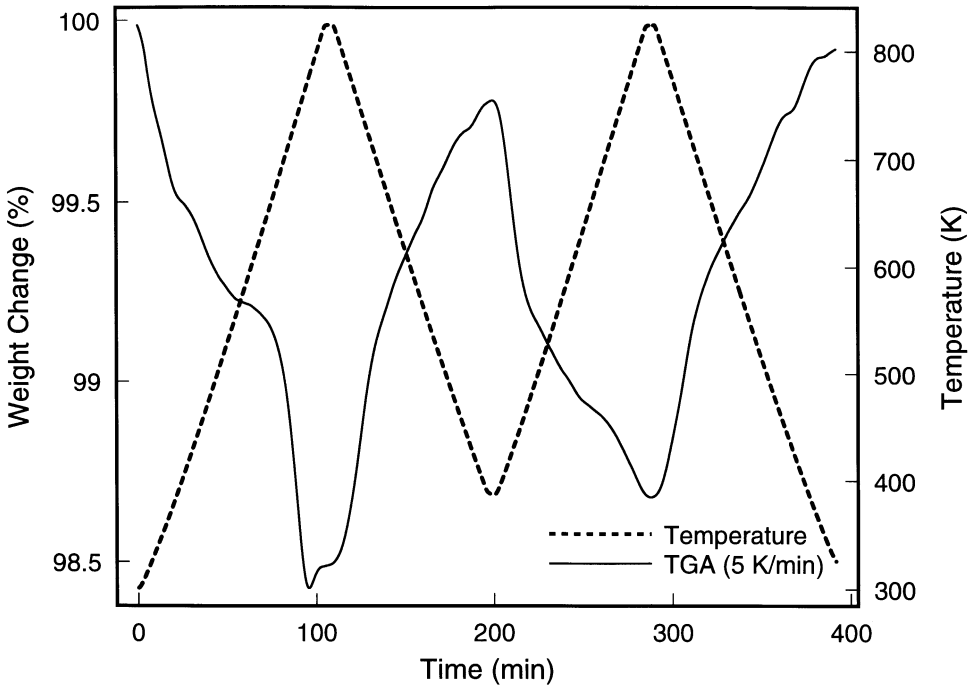

Figure 1. Cyclic TG-IMR-MS experiment with the catalyst in nitrogen during heating and in synthetic air during cooling down. The oscillations in weight became gradually featureless and smaller in amplitude. The frequency of the weight changes increased over that of the temperature oscillation indicating an increase in the reaction kinetics. The first two oscillations are shown here in high resolution to allow the identification of structure in the weight losses relevant for the analysis of the reactions. The evolution of molecular water, of NO, ammonia and CO_2 in trace amounts was observed during the initial heating.

absorption was further interfering resulting in a loss of complete reversibility (see, e.g., first and second weight loss profile). The loss curve between 400 and 600 K was integrated and found to correspond to 0.1 formula unit of oxygen referring to the title composition. This fraction is considered as the pumping capacity of the material under the kinetic conditions given.

Several temperature-programmed experiments were carried out in order to find out about the different reactions indicated by the stepped weight loss profile in figure 1. A compilation of the results is presented in figure 2, where arbitrary ordinate scales are used in order to show the qualitative relations. The two DSC experiments revealed that the catalyst was metastable in air with respect to an irreversible structural phase transition. The double exothermic signals were ascribed to a final oxidation of residual ammonia at 695 K (113.7 mJ/mg) and to the intrinsic phase transition at 781 K (18.2 mJ/mg). All further experiments were thus halted at 730 K in order not to trigger the structural phase transition.

A series of TPD experiments with slow heating rates and gas atmospheres of He and oxygen respectively yielded the three traces displayed in figure 2 . The reversible oxygen pumping from figure 1 was reproduced but occurred at higher temperatures than seen in figure 1. The fact that the pumping occurred overlapping with the ligand oxidation process indicated that the residual ligands of the catalyst play here the role of a reductant which would be the organic phase under steady state conditions. The observation is further in full agreement with the conjecture that a reducing agent has to activate the Mars–van Krevelen materials for oxygen pumping which is not achieved solely by thermal cycling.

A TDS experiment in UHV gave at slow heating rates a broad signal beginning at around 400 K and not terminating at the phase transition temperature. Sub-surface diffusion (see figure 1) prevented a useful interpretation of this surface-sensitive experiment. A discernible signal peaking at 500 K was obtained by subtracting the background signal.

The grey area in figure 2 marks the useful temperature range for catalytic operation. All signals showed some contribution in this area allowing to conclude that subsurface activation of oxygen plays indeed a role in the catalytic action of the material. The upper limit of the temperature window of activity was lower than the beginning of the structural rearrangement which occurred independently from the residual oxidation of ammonia ligands. This means that the structurally metastable state of the material is the catalytically active phase.

The TDS peak at 500 K cannot be ascribed to surface atomic oxygen as the ISS experiment ruled out its existence. It is ascribed to the desorption of the active lattice oxygen species. To support this assignment the TDS signal is compared in figure 3 to the IMR-MS responses of several subsequent TPO runs performed at atmospheric

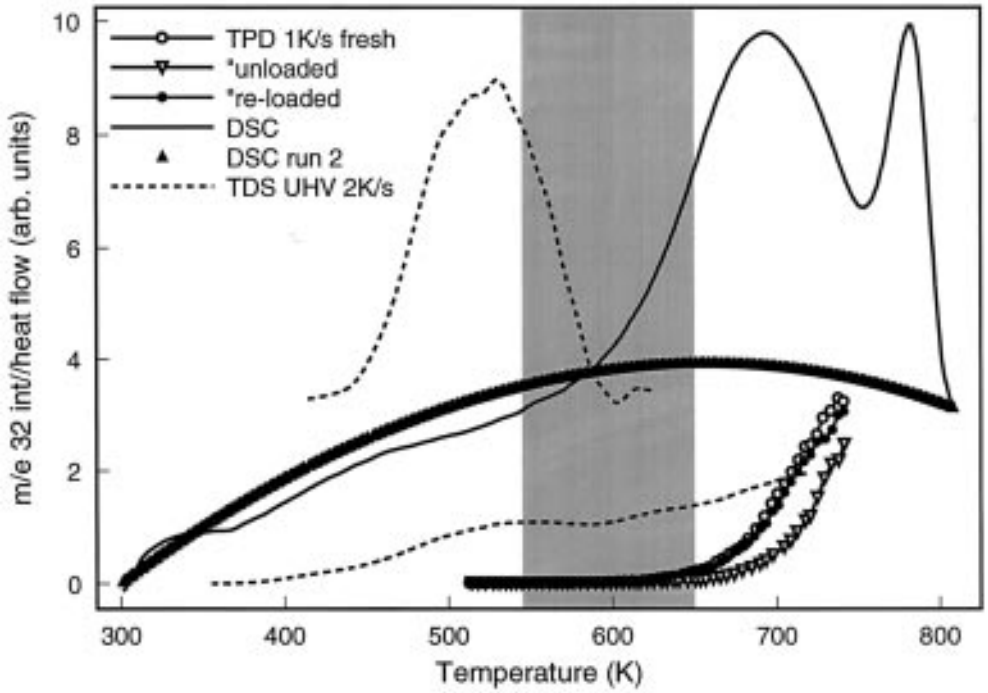

Figure 2. Compilation of temperature-programmed signals of the catalyst. The DSC was run in air with a reference signal from SiC (heating rate 5 K/min). The TPD runs (lines with symbols) were performed in a quartz microreactor coupled to a quadrupole MS. Desorption was done in 50 mbar He with external heating, oxygen loading was achieved with 50 mbar oxygen with also external heating. The TDS experiments were performed with the samples used for surface analysis on a gold substrate with internal heating.

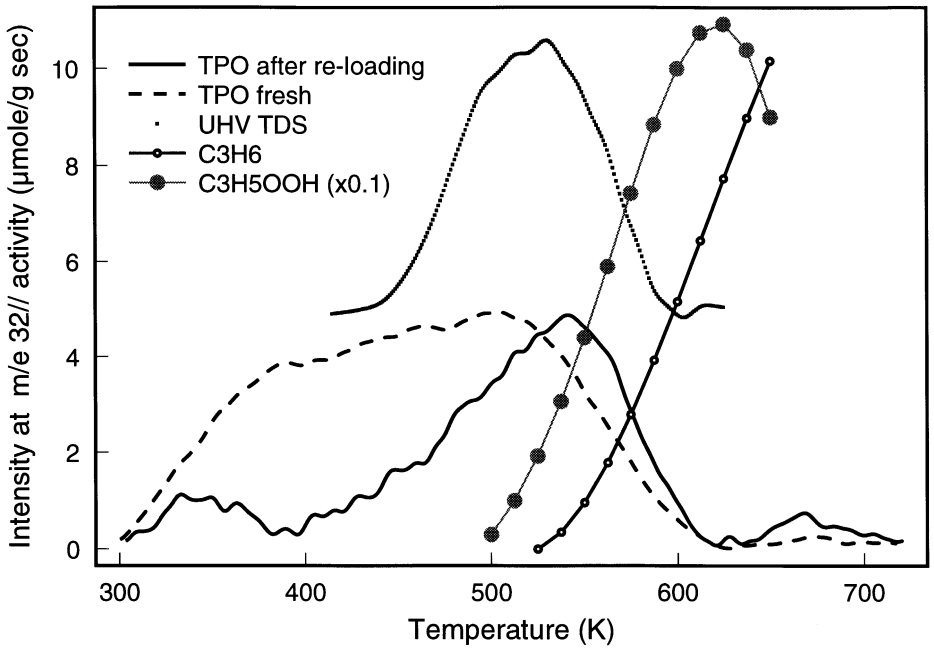

Figure 3. Comparison between various temperature-programmed desorptions of oxygen and the stationary catalytic activity in selective oxidation of *n*-propanol. The IMR-MS detector allowed to follow the reaction pathways to propene, propionic acid via propionaldehyde, and deep oxidation simultaneously with a time resolution of 5 s. The total conversion was about 5.6% with a 80% contribution of propene at 623 K. The TPO signal between 300 and 400 K is due to surface species as it scales with the BET surface area of the catalyst (varied between about 2 and 10 m^2/g for different batches). The large difference in TPO signals between as-prepared and second loading stages is due to oxygen consumption for oxidation of ammonia to NO and water.

pressure. The IMR-MS traces ensured that after the first oxidation yielding the broad response in subsequent runs no oxygen was consumed for residual ligand oxidation. The good agreement between the TDS peak and the TPO response indicates indeed that the origin of the desorbing oxygen is not the surface but the bulk of the catalyst material. The analysis agrees further well with the assignment of the step structure of the weight loss in figure 1 confirming the estimation of the oxygen pumping capacity of the catalyst.

The result of a differential conversion test with *n*-propanol/water is also shown in figure 3. The data indicated that the interaction of the active oxygen with the catalyst was not perfectly matching the requirement for the catalytic conversion of the substrate as a major fraction of the peak area fell outside the temperature window of catalytic activity. The data implied that the selective oxidation activity should be limited in the present case by the availability of lattice oxygen at high temperatures and by the activation of the substrate at low temperatures. The conversion data showed also that the two functions of the oxide catalyst, namely acidity (leading to propene) and oxidation (leading to propionic acid via propione aldehyde), operated independently from each other. An influence of the different kinetic conditions (stationary conversion vs. temperature-programmed oxidation) is considered unlikely as the variation of the heating rate from 1 K/s (TDS) to 0.085 K/s (TPO) gave a significantly smaller displacement than the disagreement between the desorption and conversion curves.

3.3. The electronic structure

The catalyst was a zero-gap semiconductor allowing to record photoemission spectra in all energy ranges without charging problems. Within the valence band the spectral weight of the metal d states is 11% for He I and 21% for He II radiation. For this reason the He II data were shown in figure 4. The spectrum was characterised by a broad three-peak structure in the central range and a weak signal at low energy. The arrows in figure 4 mark the positions of the three prominent and well-split peaks in the valence band spectrum of the basal plane (010) of single crystalline MoO_3 [15] . The positions agreed but the much wider lines in the present case indicated a lowering of the octahedral symmetry of the MO_6 octahedra which resulted in a loss of degeneracy in the ligand field [16] and hence in a broadening of the photoemission signals. This would be fully compatible with a partial reduction of the metal ions causing the population of metal d states which are empty for formal Mo^{6+} ions.

The weak structures below 3 eV arise from band gap states in the MoO_3 structure and are of predominantly Mo 4d character [15] . The photoemission from the V^{4+} ions which was not discernible in the main peak will also contribute to the band gap states which indicated by their total intensity the degree of chemical reduction of the oxide.

The first five spectra showed the effects from two successive unloading and reloading cycles corresponding to the TPD experiments in figure 2. No strong features of

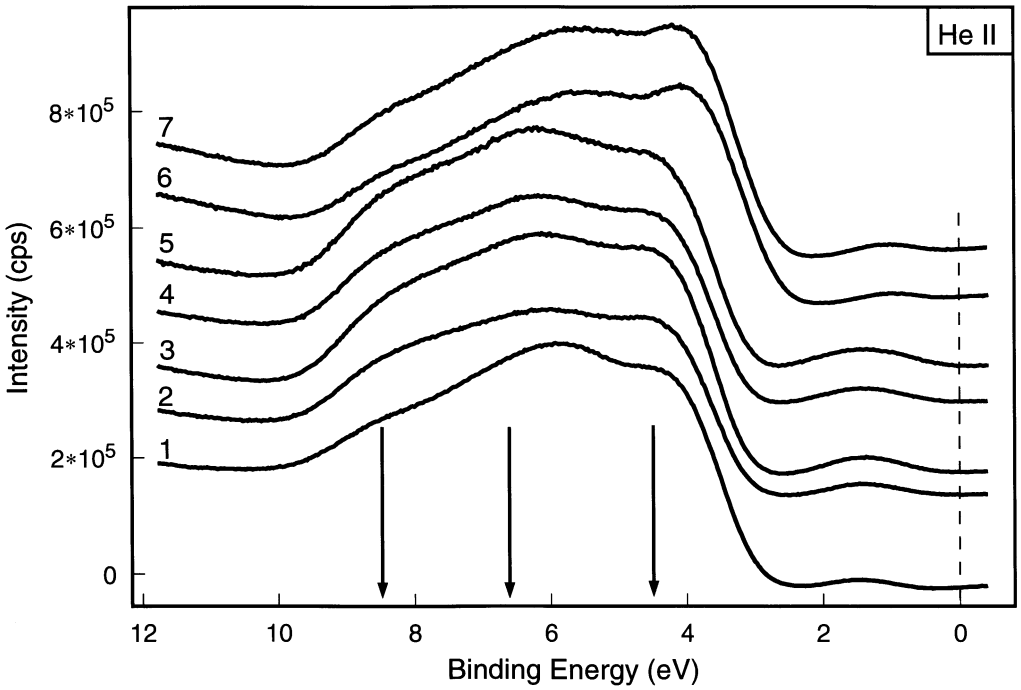

Figure 4. He II UPS (40.8 eV) valence band data for the catalyst after various treatments: traces 1, 3 and 5 represent oxygen-loaded forms, traces 2 and 4 the corresponding unloaded forms for a maximum treatment temperature of 730 K. Traces 6 and 7 were recorded after an unloading–loading cycle up to 800 K which caused an irreversible change in the spectrum. The dashed line denotes the Fermi energy (by calibration with gold), the arrows indicate positions of prominent peaks in the spectrum of a MoO_3 single crystal (see text).

chemisorbed atomic oxygen (peak between 4.5 and 6.5 eV) occurred upon reloading. The unloaded states (spectra 2 and 4 in figure 4) were still broader in their main features indicating an additional element of structural distortion in the unloaded state. The spectra 6 and 7 resulted from an unloading and reloading cycle at 800 K, which is above the structural phase transition temperature. This transition manifested itself in a qualitative change of the spectrum. The symmetry of the MO_6 octahedra has changed again and the overall similarity to the spectrum of MoO_3 was significantly reduced. The data confirmed the thermochemical bulk data for the surface of the catalyst namely that oxygen pumping is reversible up to 750 K but irreversibly changes the electronic structure when the temperature is raised to 800 K. Again no sign was found for a layer of surface adsorbed oxygen.

The question about the oxidation state of the catalyst during oxygen pumping was followed in detail by inspection of the band gap states [15]. The relevant sections from the He I data which are free of satellite artefacts are displayed in figure 5. Unloading of the material caused the intensity of the reduced states to increase. Reloading, which was successful as seen from the TDS spectrum in figure 2 caused a reduction of the intensity of the spectrum in an energy range between 0.5 and 2.1 eV. Subsequent loading–unloading cycles showed this intensity change to be reversible. An irreversible oxidation (loss in intensity) occurred after a loading cycle at 800 K. It is evident that a contribution around 1 eV below the Fermi energy remained unaffected and that oxidation occurred predominantly in the energy range where the intensity changes associated with the reversible oxygen loading were observed. These data directly confirmed the conjecture that some reduced Mo centres ("defects") were responsible for the oxygen pumping in the active catalyst [9,17]. It is pointed out that these centres were extrinsic to the structure of Mo_4VO_{14} and were formed only during the autoreduction conditions of the calcining step of the catalyst material. These active centres were greatly reduced in abundance during the structural phase transition which is in line with the absence of a DSC effect under non-oxidising conditions. The structurally disordered state of the catalyst contained a maximum of the reduced sites involved with the oxygen pumping.

3.4. Structure by X-ray diffraction

The X-ray diffraction pattern of the active catalyst consisted of a diffuse background pattern with one prominent sharp line at $d = 0.399$ nm and its weak second order peak [8,7]. In situ X-ray diffraction revealed the phase to be stable up 873 K in high vacuum or in nitrogen atmospheres. Under oxygen, however, the material recrystallised at 773 K into a highly crystalline phase of Mo_4VO_{14}. The JCPDS file (31-1437) and the corresponding single-crystal structure were obtained from a sample with only 7 at% vanadium compared to the present material with 20 at% vanadium. Consequently, the

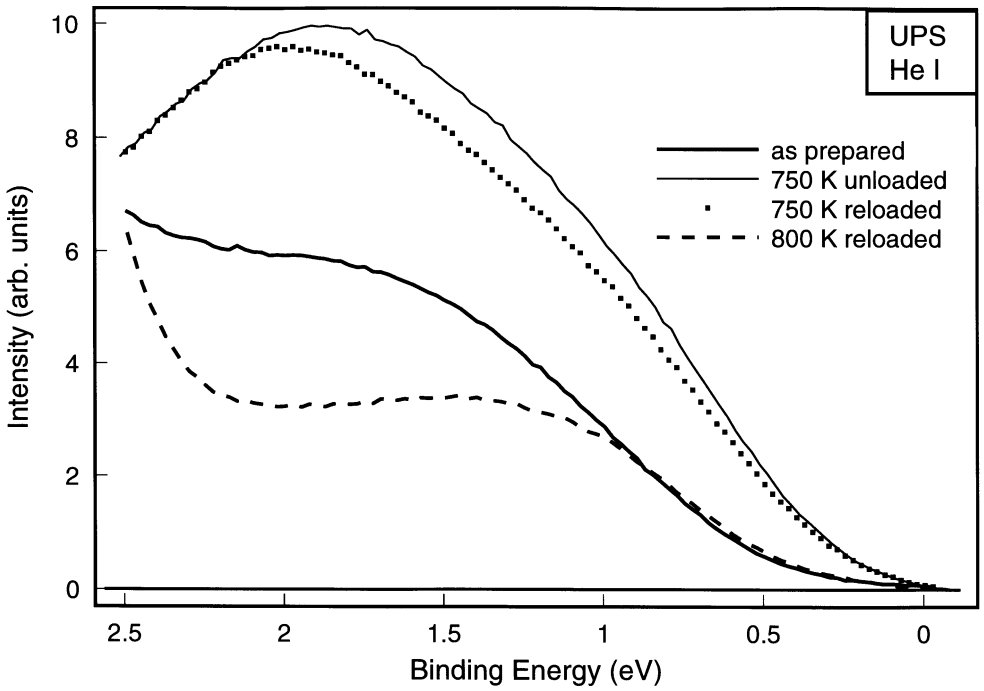

Figure 5. Section of the He I UPS data showing the band gap states close to the Fermi level. The catalyst is at all stages a zero-band semiconductor, as can be seen from the spectral intensity ranging down to 0.0 eV. The very weak background of He I satellites is not detected here due to the absence of sharp features in the main spectrum. All spectra were normalised to a point close to 10 eV binding energy.

lattice parameters of the present crystalline phase were slightly different. The material crystallised in a tetragonal system with the (001) reflection being the 100% line at $d = 0.399$ nm, exactly at the position where the single line was found in the nanocrystalline state.

The structure is isotypic to the Mo_5O_{14} structure (space group P4/mbm, $a = b = 2.3000$ nm, $c = 0.3937$ nm) which is shown as polyhedral representation in figure 6. In the *a–c* plane (prismatic face) the structure consists of layers of corner-sharing octahedra. No edge-sharing occurs in this plane, much in contrast to the parent MoO_3 structure which consists of layers of edge-sharing double octahedra. In the *a–b* plane (basal plane) the structure is very loosely packed and consists of clusters of octahedra around a fivefold bipyramid containing a lower valent (e.g. Mo^{5+}, V^{4+}) metal atom. The clusters are interconnected by a network of corner-sharing octahedra giving rise to a high in-plane mobility of the basic structural units and to the formation of channel network suitable to accommodate heteroatom dopants (as in the multi-element oxide technical catalysts) and for oxygen. Closer inspection of the octahedra reveals that they are significantly distorted with respect to the M–O bond distances in axial as well as in equatorial directions. The metal atom is displaced from the centre of the polyhedron.

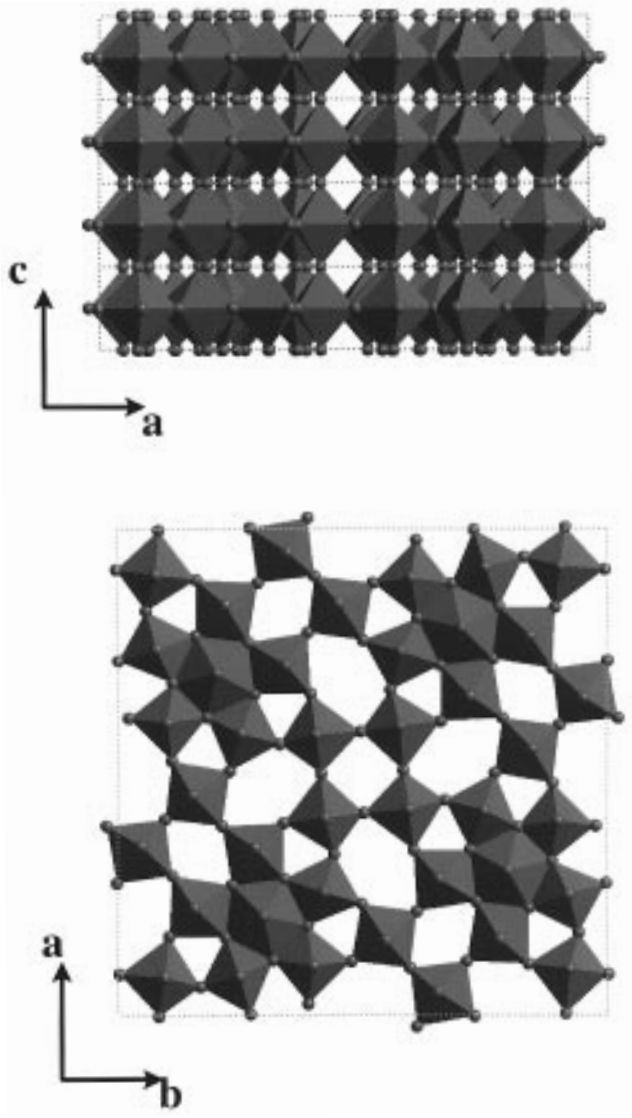

Figure 6. Polyhedral representation of the Mo_4VO_{14} structure. Top: prismatic face, bottom: basal plane views. The basal plane structure is composed of chains running diagonal to the plotted section holding the clusters of polyhedra together. Loosely connected squares of basic structural units fill the voids between the chains and the clusters (centre of the plotted section).

When during oxygen pumping (figure 1) a metal centre is reduced in its valent state the distortions will increase and favour edge-sharing in order to allow for the covalent M–O–M interaction which is well-known in Mo-bronzes. These findings are in good agreement with the discussion of figure 3. Re-oxidation reduces the d-band occupation and thus allows the electrostatic repulsive interaction between highly charged metal centres to take command over the structure preferring the maximum-distance corner-sharing connectivity [10,9].

3.5. Structure by electron microscopy

The nanocrystalline state of the catalyst was investigated by HRTEM in order to probe directly the connectivity of the octahedra. The results were summarised in figures 7 and 8 . The survey in figure 7 revealed clearly the anisotropy in long range ordering. Electron diffraction of the material resulted in perfectly continuous ring patterns (*d* spacing: 0.39 nm sharp, 0.34 nm diffuse, 0.18 nm diffuse and 0.13 nm diffuse). In full agreement with the XRD pattern the presence of stacks of diffraction planes with a distance of 0.4 nm was clearly detectable. The material was due to in-plane disorder nanocrystalline with crystallite sizes below 10 nm. The grain boundaries are frequently intergrown with the misfits being compensated in small areas of complete structural disorder (no contrast). A small section of such an interface area was imaged in figure 8A. The top left side showed the 0.39 nm spacing terminating in a diagonal line to a crystallite oriented with its basal plane towards the electron beam. In this area the complex connectivity resulting in a poorly ordered appearance can be seen. The situation was similar in figure 8B where the *a–b* planes of the oxide were packed in triple layers (thickness 1.2 nm).

Figure 8C was obtained using the technique of computer-simulated dark field imaging. A continuum random network of basic structural units (distorted octahedra) was detected made up from approximately circular clusters (“holes” in figure 8C) embedded in a defective quadratic network. The similarity of the arrangement to the idealised structure in figure 5 was obvious. The close-ups of figures 8D and 8E showed ring structures and their interconnection in the octahedral

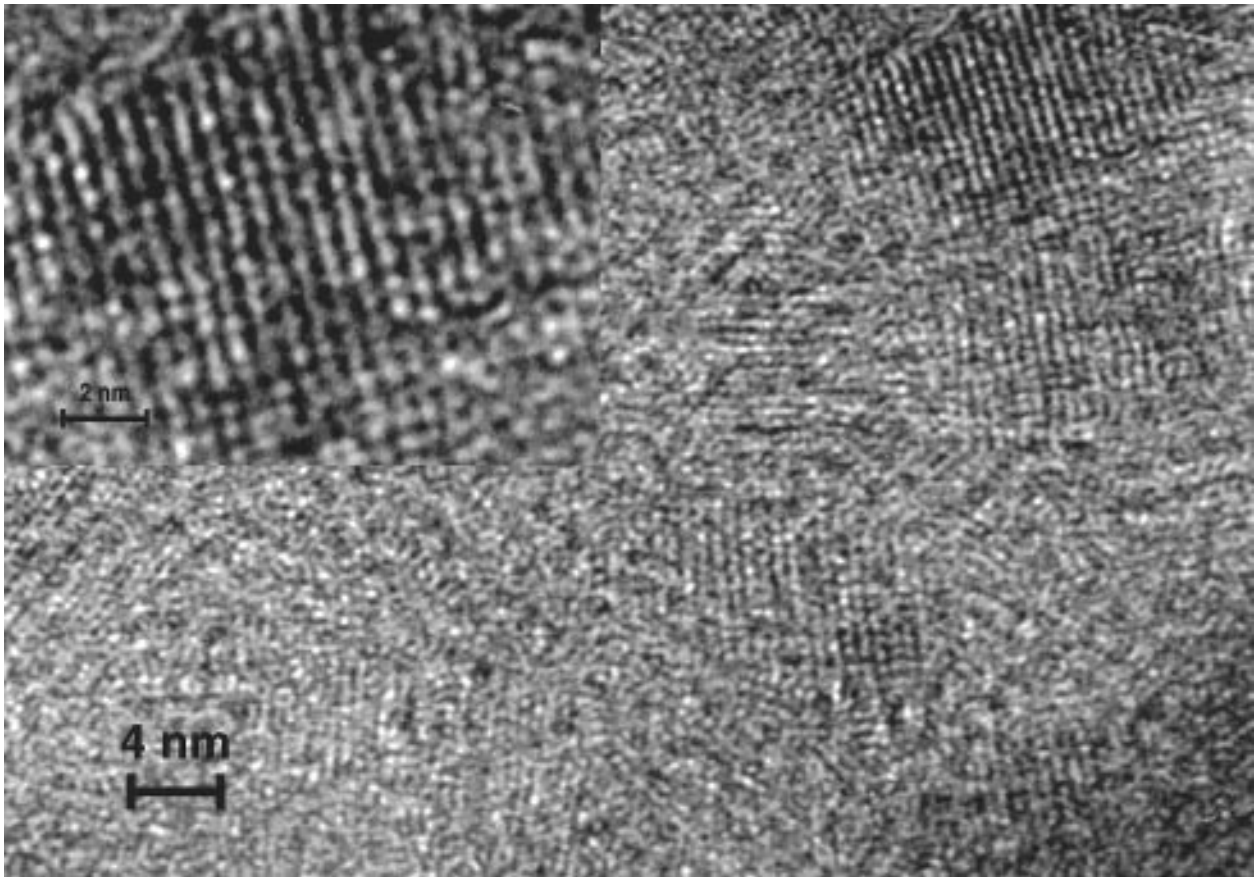

Figure 7. HRTEM image of a catalyst platelet. The microstructure of the material consists of spherical aggregates of platelets allowing direct imaging without thinning. The inset shows a close-up on an area exhibiting a prismatic face of a well-stacked nanocrystal (compare to top view in figure 5).

network. The extremely complex structure in these images prevented the application of computational methods for contrast analysis and thus did not allow to assign the contrast to holes and octahedra as it might be done by intuition. It remained a speculation that the ring structures were caused by partly reduced metal atoms and hence would represent the active centres in catalysis.

4. Conclusions

The set of complementary experiments revealed the following general picture of the active catalyst. The function of oxygen pumping was demonstrated experimentally in a partially reduced oxide phase. This was also observed in earlier model studies with a single crystal of MoO_3 [17]. The optimum temperature for the oxygen pumping did not match (figures 2 and 3) the optimum temperature for the activation of the substrate. A better match between the two temperatures (energetics) is required as one optimisation strategy for the catalyst. The activation of the substrate and influences of surface acidity need to be evaluated in detail.

The kinetics of the oxygen pumping driven by temperature gradients was slow on a timescale of minutes. Instationary experiments [18] have to reveal the kinetics driven by gradients of chemical potential (consumption by reaction under isothermal conditions). In this respect the results presented were model experiments with an unknown quantitative relation to the stationary case (figure 3).

The active phase was found to be a nanocrystalline variety of the long range order phase Mo_4VO_{14}. The disorder was characterised by two elements. A small average crystallite size paired with an anisotropic shape of the crystallites gave rise to a large grain boundary internal surface area. The substitution of Mo^{6+} by V^{4+} and $Mo^{(6-x)+}$ centres created additional asymmetry in the octahedral building blocks and required a variety of cross-linking patterns to maintain electroneutrality, to accommodate the metal–metal interactions and to minimise internal strain.

The structural motif of the catalyst material (figure 6) was characterised by a strong anisotropy of the arrangement of the building blocks giving rise to dense layers in the (010) direction and very open structures in the (001) plane. The open structure allowed to accom-

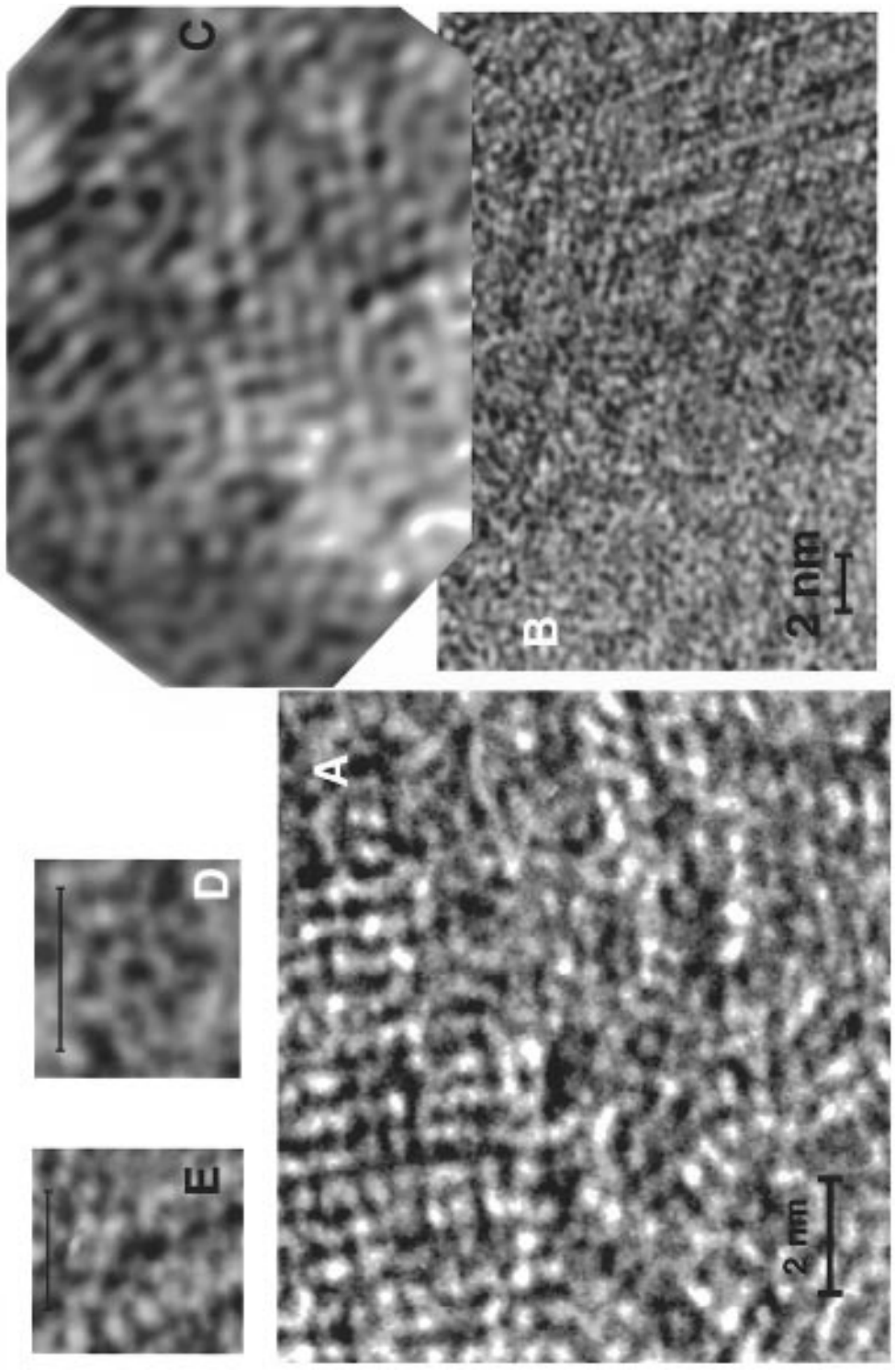

Figure 8. Collection of HRTEM images of the nanocrystalline phase at grain boundaries exposing in each plate part of the basal plane view. The significant disorder in the connectivity compared to the arrangement shown in figure 5 (bottom) can be seen. For a detailed explanation see text.

modate the substitutional modifications caused by the defects without a large sacrifice in energy keeping the nanocrystalline state of the material metastable up to temperatures useful for catalytic activation of the substrates.

The oxygen pumping function (figure 1) is considered on an atomic level as a motion of octahedral units changing reversibly their cross linking [9,10]. It is obvious that the activation energy of this motion and hence the reaction kinetics is optimised if the movements are decoupled in space and time, i.e. if the units can change their cross-linking pattern independent of each other. The more reduced the co-operativity of the structure will be (avoiding edge-sharing connectivity), the more favourable will this be for the kinetics. In this respect the present structure is superior to conventional shear structures discussed in the literature [9,12,10] as they require co-operative movement of chains of building blocks. The lower boundary condition for breaking the co-operativity is, of course, to preserve the basic structure and to prevent phase separation or crystallisation. In this respect the layer motif with the strong anisotropy of the cross linking in different directions of the Mo_4VO_{14} structure (figure 6) is highly desirable. The most useful structural motif for a maximum flexibility of the basic structural units to change their connectivity is the transformation of the Mo_4VO_{14} basal planes into a two-dimensional disordered phase. In such an arrangement constituting a two-dimensional glass, a maximum number of local arrays exists in which translations or rotations of individual octahedra can contribute to the oxygen pumping. Such a structural disposition was made visible in the real catalyst system (figures 7 and 8). The constitution of each glassy layer of similar basic structural units ensures frequent matching in the direction perpendicular to the layer and allows thus for chemical cohesion of the crystallite (figures 6 and 8A).

The ''defects'' in a multicomponent oxide catalyst [19,10,9] reduce the connectivity of the octahedra and help greatly to start the oxygen pumping. The distortion of octahedra by metal substitution or by reduction of the formal oxidation number as evidenced by the valence band electronic structure (figure 4) further helps to break up the cross linking. The introduction of clusters of octahedra within a corner-sharing network allows to optimise the functions of charge acceptance (from the organic substrate) by maximising the vanadium content and of oxygen pumping by substitution of molybdenum by tungsten. WO_6 octahedra will stabilise the corner-sharing connectivity due to electrostatic interaction of the metal centres and so prevent agglomeration of the cluster units. These parameters can be used to optimise the loosening of the connectivity within the limits of the phase stability. Within this picture it becomes apparent why it is useful to create a chemically complex multi-element oxide and to optimise the calcination/reduction procedure as these are the practical tools for the adaptation of the system to specific catalytic requirements.

The large internal surface area of the nanostructure increases the activation energy for the ordering phase transition. The size of the crystallites is optimum when the decay of the gradient of the oxygen ionic conductivity (which is needed to use the lattice oxygen for catalysis) is about half of the crystallite diameter. Such engineered ''heterogeneously doped'' ionic conductors have been developed and thoroughly analysed in halide systems and the beneficial effect of nanosize optimisation in conducting oxides [20] has been confirmed experimentally and theoretically [21]. This optimisation accelerates the kinetics of lattice oxygen motion and hence affects directly the catalytic performance. The limit of optimisation is again maintenance of the dimensional stability of the nanoscale system under steady state conditions.

The positive proof for a glass-like active catalyst phase allows the applications of Zachariasen's theory of glass formation [22] to predict the parameter space for optimisation. First we note that the distortion of the MO_6 octahedra is prerequisite for glass formation within the rules of Zachariasen. The synergy effects documented in this particular system and in many closely related systems by addition of other oxides can be rationalised in a structural sense as follows. The oxygen donor species in the remote control hypothesis may not donate spillover oxygen atoms as controlling agents for lattice oxygen conversion but may react as continuum random network modifiers in the sense of Zachariasen and hence activate in situ the turnover of lattice oxygen by direct structural interaction. Under reaction conditions the resulting metastable systems would represent one continuous glassy system which undergoes partial or complete re-crystallisation during catalyst ageing or during shut-down and hence remain undetected in a post-mortem analytical study. The network modifiers would also optimise the site isolation and the M–O bond strength [9] of the active centres.

The prediction would be that tetrahedrally co-ordinated and chain-forming compounds would be highly effective as network modifiers which fits well with the experimental hitlist of oxygen donor species in the remote control hypothesis. In this present speculation the existence of several distinct phases and the exchange of hot oxygen atoms between them would be unnecessary to explain the synergy of mixing certain oxides with the oxygen pumping matrix.

Finally it is pointed out that the process of selective oxidation requires additional ''jobs'' of the catalyst to be performed which are not mentioned here. The above findings allow thus only to discuss part of the mode of action of a multi-element selective oxidation catalyst.

Acknowledgement

The work was financially supported by the BMBF through its catalysis programme. We are indebted to the members of the collaborating groups of Professors Gaube, Vogel and Linz for numerous discussions.

References

[1] V.C. Malshe and S.B. Chandalia, J. Appl. Chem. Biotechnol. 27 (1977) 575.
[2] M. Ai, Appl. Catal. 27 (1986) 167.
[3] T.V. Andrushkevich, Catal. Rev. Sci. Eng. 35 (1993) 213.
[4] J. Tichý, J. Kustka and J. Machek, Coll. Czech. Chem. Commun. 48 (1983) 698.
[5] J. Tichý, J. Kustka and J. Vencl, Coll. Czech. Chem. Commun. 39 (1974) 1797.
[6] S. Breiter, M. Estenfelder, H.-G. Lintz, A. Tenten and H. Hibst, Appl. Catal. A 134 (1996) 81.
[7] T.V. Andrushkevich, V.M. Bondareva, G.Ya. Popova and L.M. Plyasova, in: *New Developments in Selective Oxidation by Heterogeneous Catalysis*, Stud. Surf. Sci. Catal., Vol. 72, eds. P. Ruiz and B. Delmon (Elsevier, Amsterdam, 1992) p. 91.
[8] L.M. Plyasova, L.P. Solov'eva, G.N. Kryukova and T.V. Andrushkevich, Kinet. Catal. 31 (1990) 1253.
[9] R.K. Grasselli and J.D. Burrington, Adv. Catal. 30 (1981) 133.
[10] L.T. Weng, P. Ruiz and B. Delmon, in: *New Developments in Selective Oxidation by Heterogeneous Catalysis*, Stud. Surf. Sci. Catal., Vol. 72, eds. P. Ruiz and B. Delmon (Elsevier, Amsterdam, 1992) p. 399.
[11] O. Legendere, Ph. Jaeger amd J.P. Brunelle, in: *New Developments in Selective Oxidation by Heterogeneous Catalysis*, Stud. Surf. Sci. Catal., Vol. 72, eds. P. Ruiz and B. Delmon (Elsevier, Amsterdam 1992) p. 387.
[12] J.D. Burrington, C.T. Kartisek and R.K. Grasselli, J. Catal. 87 (1984) 363.
[13] E.M. Al'kaeva, T.V. Andrushkevich, O.Y. Ovsiter and V.D. Sokolovskii, Catal. Today 24 (1995) 357.
[14] R. Recknagel and L. Riekert, Chem. Technik 46 (1994) 324.
[15] L.E. Firment and A. Ferretti, Surf. Sci. 129 (1983) 155.
[16] G. Mountjoy, J. Yuan and P.H. Gaskell, Inst. Phys. Conf. Ser. 138 (2) (1993) 35.
[17] J. Haber, W. Marczewski, J. Stoch and L. Ungier, Ber. Bunsen-Ges. 79 (1975) 970.
[18] U.S. Ozkan, S.A. Driscoll, L. Zhang and K.L. Ault, J. Catal. 124 (1990) 183.
[19] M.D. Allen, S. Poulston, E.G. Bithell, M.J. Goringe and M. Bowker, J. Catal. 163 (1996) 204.
[20] F. Noll, W. Münch, I. Denk and J. Maier, Solid State Ionics, in press.
[21] J. Maier, Prog. Solid State Chem. 23 (1995) 171.
[22] S.R. Elliot, *Physics of Amorphous Materials* (Longman, London, 1983) pp. 40ff.